Estimating material viscoelastic properties based on surface wave measurements: A comparison of techniques and modeling assumptions

Thomas J. Royston[a] and Zoujun Dai
Department of Mechanical and Industrial Engineering, University of Illinois at Chicago, 842 West Taylor Street MC 251, Chicago, Illinois 60607

Rajesh Chaunsali
Department of Mechanical Engineering, India Institute of Technology, Madras Chennai 600 036, India

Yifei Liu and Ying Peng
Department of Mechanical and Industrial Engineering, University of Illinois at Chicago, 842 West Taylor Street MC 251, Chicago, Illinois 60607

Richard L. Magin
Department of Bioengineering, University of Illinois at Chicago, 851 South Morgan Street MC 063, Chicago, Illinois 60607

(Received 1 August 2011; revised 3 October 2011; accepted 4 October 2011)

Previous studies of the first author and others have focused on low audible frequency (<1 kHz) shear and surface wave motion in and on a viscoelastic material comprised of or representative of soft biological tissue. A specific case considered has been surface (Rayleigh) wave motion caused by a circular disk located on the surface and oscillating normal to it. Different approaches to identifying the type and coefficients of a viscoelastic model of the material based on these measurements have been proposed. One approach has been to optimize coefficients in an assumed viscoelastic model type to match measurements of the frequency-dependent Rayleigh wave speed. Another approach has been to optimize coefficients in an assumed viscoelastic model type to match the complex-valued frequency response function (FRF) between the excitation location and points at known radial distances from it. In the present article, the relative merits of these approaches are explored theoretically, computationally, and experimentally. It is concluded that matching the complex-valued FRF may provide a better estimate of the viscoelastic model type and parameter values; though, as the studies herein show, there are inherent limitations to identifying viscoelastic properties based on surface wave measurements. © *2011 Acoustical Society of America*.
[DOI: 10.1121/1.3655883]

PACS number(s): 43.80.Cs, 43.80.Ev, 43.20.Jr [CCC] Pages: 4126–4138

I. INTRODUCTION

An improved understanding of surface (Rayleigh) wave motion on a viscoelastic material is essential to developments in many areas including medicine, geophysics, infrastructure and manufacturing. For example, in medical diagnostics research, linear surface *and* shear wave behavior—phase speed and attenuation rate—on and in soft biological tissues have been studied extensively as this behavior can be significantly altered by changes in the shear elasticity and viscosity of the tissue caused by various pathologies, trauma or remodeling.[1–3] For soft biological tissues (e.g., comparing muscle with fat), the x-ray attenuation coefficient varies only by a factor of 2,[4] while MR relaxation times vary by a factor of 3.[5] The shear moduli, on the other hand, can vary by more than a factor of 10, potentially providing greater contrast.[6–8]

Understanding shear wave behavior is key to dynamic elastography techniques that use magnetic resonance imaging (MRI) or Doppler ultrasound (US) procedures to generate images of the shear wave field. Surface wave behavior, measured via optical or Doppler US methods, has also been studied for the same reasons. A thorough understanding of surface *and* shear wave behavior on the same soft tissue phantom can be useful in cross-validation of the various elastography and surface measurement techniques, given their similar dependence on shear viscoelastic properties.

A range of viscoelastic constitutive models have been proposed to interpret shear and surface wave measurements. These models attempt to relate measurable phenomena to the underlying elasticity and damping of the material, both of which are typically rate- (frequency-) dependent. Historically, many studies have often assumed a Voigt model of

[a]Author to whom correspondence should be addressed. Electronic mail: troyston@uic.edu

viscoelasticity. Recent studies have shown that such models have limitations in their ability to accurately capture dynamic phenomena over multiple time scales and/or with broad spectral content, particularly for biological tissues and tissue mimicking phantoms. One way to overcome such limitations is through the use of more complex models with a larger number of parameters to optimize; another approach is via fractional order models.[9–14] Fractional order viscoelastic models have shown the potential to yield new disease and treatment specific parameters that more effectively predict underlying changes in tissue associated with developing pathology, such as liver cirrhosis and breast cancer. As an example, in Ref. 14 a relatively simple power law relationship was fit to the complex shear modulus of human breast tissue and tumors measured by magnetic resonance elastography. The results, when plotted as the fractional power exponent versus the fractional order attenuation, separated benign from malignant tumors with an increase in specificity and sensitivity.

In previous studies of the first author of the present article[15,16] there has been an emphasis on understanding the surface wave field created in a material like biological tissue by canonical vibratory sources. In Ref. 15, a new analytical solution was derived for the problem of surface wave generation on a linear viscoelastic half-space caused by a finite rigid circular disk located on the surface and oscillating normal to it. While the motivation of the work was to better understand surface wave propagation in biological tissue, the solution approach taken was an incremental advancement of theoretical work reported in seminal articles in the geophysics literature.[17,18] The improved solution was tested experimentally using a viscoelastic phantom with material properties comparable to biological soft tissue. Some agreement could be achieved over a limited frequency range (20–100 Hz) using a Voigt model. In a more recent study revisiting the same canonical system on a different phantom material it appeared that an improved match could be achieved over a broader frequency range by using a fractional order viscoelastic model.[19]

In these studies of the first author, the approach was to measure the complex-valued frequency response function (FRF) between the excitation location and points at known radial distances from the excitation location. The FRF has embedded in it frequency-dependent information about both surface wave phase speed and attenuation that can be used to directly estimate the real and imaginary parts of the complex shear modulus (storage and loss shear moduli). The coefficients in an assumed viscoelastic tissue model type can then be optimized to minimize the differences in the predicted and experimentally determined values of the complex shear modulus. Another approach taken by others has been to directly estimate the frequency-dependent surface (Rayleigh) wave speed from experimental data and then to optimize the coefficients in an assumed viscoelastic model type to minimize the difference between the measured and predicted values of wave speed.[3,20–22] In an analogous manner, *shear* wave speed dispersion derived from elastography techniques has been used to estimate the shear viscoelasticity with an assumed viscoelastic model type.[23–29] In the present article, the relative merits of these approaches are explored theoretically, computationally, and experimentally.

II. VISCOELASTIC CONTINUUM: GOVERNING EQUATIONS

For an isotropic, homogenous, viscoelastic compressible medium one can use the following formulation of the equation of motion for small perturbations about an operating point

$$(\lambda+\mu)\nabla\nabla\cdot\mathbf{u}+\mu\nabla^2\mathbf{u}=\rho\frac{\partial^2\mathbf{u}}{\partial t^2}. \tag{1}$$

Here, $\mathbf{u}$ is the displacement vector, ρ is the density of the medium, $\partial/\partial t$ denotes a derivative with respect to time, ∇ is the spatial Laplacian operator dependent upon the chosen coordinate system, and λ and μ are the Lame constants of the medium. For a linear viscoelastic Voigt material model, the rate-dependent Lame "constants" are expressible as $\lambda(t)=\lambda_0+\lambda_1\partial/\partial t$ and $\mu(t)=\mu_0+\mu_1\partial/\partial t$ where λ_0, λ_1, μ_0, and μ_1 are coefficients of volume compressibility, volume viscosity, shear elasticity, and shear viscosity, respectively.[30] Other shear viscoelastic models will lead to different rate-dependence relations.

With regard to μ, it has been observed in many materials that the simple two-element Voigt model for shear viscoelasticity (μ_0, μ_1) does not accurately capture material shear dynamic behavior, in terms of its experimentally-measured response to various elementary excitation waveforms, such as step inputs or periodic or random inputs with broad spectral content. More complex arrangements of multiple elastic (springs) and viscous (dashpot) components may then be employed empirically in order to more closely match what is observed. For example, the Standard Linear Solid (SLS) Model, also known as the Kelvin or Zener model, consists of a parallel combination of a Maxwell element (spring and dashpot in series) with a spring. The three-element SLS model has more flexibility in representing dynamic viscoelasticity as compared to the Voigt model.[7] Instead of increasing the constitutive model complexity by increasing the number of components that comprise it, an alternative is to consider that the material may exhibit rate-dependent shear deformation that is best described by a single element, comprised of two constants, μ_α and α, whose behavior lies somewhere between Hookean solid and Newtonian fluid. Specifically, fractional order viscoelasticity (a springpot) can be specified as shown in the second term of the following:

$$\mu=\mu_0+\mu_\alpha\frac{\partial^\alpha}{\partial t^\alpha},\quad 0<\alpha\leq 1. \tag{2}$$

Equation (2) is referred to as a fractional order Voigt model for $\alpha<1$. While such a mathematical construction may seem to lack physical meaning, it can be shown that this type of relation results asymptotically when using a ladder-like fractal arrangement of integer-order elastic and viscous components, as depicted in Fig. 1.[31] Indeed, such an arrangement

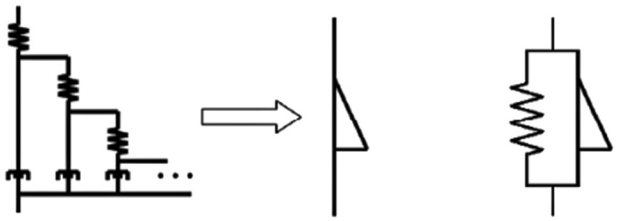

FIG. 1. A tree arrangement of springs and dashpots (left) resulting in a fractional order element, called a springpot (middle). Schematic representation of a fractional order Voigt model (right); the dashpot is replaced with a springpot.

might be rationalized on the grounds that it represents multiscale rate-dependent stress-strain interactions that one would inherently expect in some materials with complex multiscale cellular and extracellular structure, such as biological tissues. Furthermore, suitably defined fractional derivatives do not pose significant difficulty mathematically for well-conditioned functions. [In this paper we have chosen to use the Weyl definition of the fractional order derivative, which for harmonic functions such as $f(t)=e^{j\omega t}$, has the property that $\partial^\alpha/\partial t^\alpha[e^{j\omega t}]=(j\omega)^\alpha e^{j\omega t}$.] The expression in Eq. (2) is still linear in nature and thus all rules and techniques afforded such relations, such as the validity of superposition, reciprocity, the Laplace and Fourier transforms, with associated transfer and frequency response functions, are all still valid.[31–34] In the Laplace (s) and frequency ($j\omega$) domains where $j=\sqrt{-1}$ and ω is the circular frequency, Eq. (2) respectively becomes

$$\mu=\mu_0+\mu_\alpha(s)^\alpha, \tag{3a}$$

$$\mu=\mu_0+\mu_\alpha(j\omega)^\alpha. \tag{3b}$$

Note, a significant attribute of such fractional representations is that the temporal response takes on characteristics of power-law behavior as opposed to the exponential response that one obtains with the conventional Voigt representation. A power-law response in fact has been observed in a number of biological and nonbiological materials, further motivating this type of model.[10,11]

Also note that, once one is in the frequency domain, we have $\mu(\omega)=\mu_R(\omega)+j\,\mu_I(\omega)$ (storage and loss shear moduli) and both μ_R and μ_I are independent of whether the time derivative part of the Voigt model is of integer or fractional order. They are equal to μ_0 and $\omega\mu_1$, shear elasticity and shear viscosity multiplied with circular frequency, if a conventional integer order Voigt model is used. In the case of a fractional order Voigt model since $(j\omega)^\alpha=\omega^\alpha(\cos[\alpha\pi/2]+j\,\sin[\alpha\pi/2])$ the storage modulus and loss modulus are defined, respectively, as

$$\mu_R=\mu_0+\mu_\alpha\omega^\alpha\cos\left(\frac{\pi}{2}\alpha\right), \tag{4a}$$

$$\mu_I=\mu_\alpha\omega^\alpha\sin\left(\frac{\pi}{2}\alpha\right). \tag{4b}$$

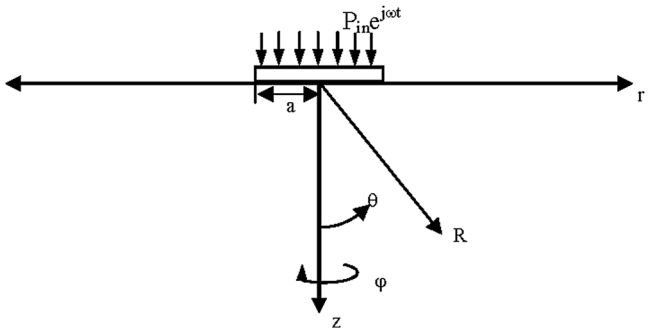

FIG. 2. Ideal viscoelastic halfspace with finite surface source.

Alternatively, the SLS model yields

$$\mu_R=\frac{\mu_0\mu_\omega^2+\omega^2\mu_1^2(\mu_0+\mu_\omega)}{\mu_\omega^2+\omega^2\mu_1^2}, \tag{5a}$$

$$\mu_I=\frac{\omega\mu_\omega^2\mu_1}{\mu_\omega^2+\omega^2\mu_1^2}. \tag{5b}$$

Here μ_0 denotes the static stiffness, μ_1 denotes the viscous damping coefficient multiplied with the first order time derivative of the displacement (thus α is equal to 1), and μ_ω denotes the dynamic stiffness, which is only effective when the loading has a non-zero time derivative.

Regardless of whether an "integer order" or fractional order Voigt model or a Standard Linear Solid model is used, wave motion in the *infinite* three-dimensional viscoelastic medium consists of a superposition of dilatational and shear wave displacements, $\mathbf{u}=\mathbf{u_P}+\mathbf{u_S}$, respectively. For the *semi-infinite* halfspace problem an additional surface (Rayleigh) wave $\mathbf{u}_{\mathrm{Su}}$ will exist.

III. SURFACE WAVE PROPAGATION ON A HALF-SPACE DUE TO A SURFACE SOURCE

In Ref. 15, a simplified analytical solution was derived for Rayleigh wave propagation on the surface of an isotropic homogeneous viscoelastic half-space caused by normal force excitation over a circular region of radius "a" on the surface of amplitude per unit area P_{in} with harmonic time dependence $e^{j\omega t}$ as depicted in Fig. 2. The analytical solution is

$$\frac{u_z}{P_{\mathrm{in}}}=-\frac{2a}{\mu}\frac{J_1(pak_p)\sqrt{p^2-1}}{F_o'(-p)}\eta^2K_0(jprk_p)e^{j\omega t}, \tag{6a}$$

where

$$F_o'(-p)=\left.\frac{\partial F_o}{\partial\zeta}\right|_{\zeta=-p}, \tag{6b}$$

$$F_o(\zeta)=\left(2\zeta^2-\eta^2\right)^2-4\zeta^2\sqrt{\zeta^2-\eta^2}\sqrt{\zeta^2-1}, \tag{6c}$$

$$\eta=\sqrt{(\lambda+2\mu)/\mu}, \tag{6d}$$

$$k_p=\omega\sqrt{\rho/(\lambda+2\mu)}. \tag{6e}$$

Here, u_z is out-of-plane surface displacement, p is the ratio of compression wave speed to surface wave speed and is a root of the function F_0 that is associated with Rayleigh wave motion, k_p is the compression wave number, r is the radial distance from center of the driving disk, J_1 is the Bessel function of the first kind (order 1), and K_0 is the modified Bessel function of the second kind (order 0); K_0 can also be written in terms of Bessel functions of the first and second kind (order 0) such as $K_0(x) = (\pi/2)i\{J_0(ix) + iY_0(ix)\}$. Equation (6c) links compression, shear and surface wave behavior to material viscoelastic properties; the roots of this equation yield compression, shear and surface wave numbers, which are complex-valued for a viscoelastic material, due to its rate-dependent stress-strain behavior.

Shear wave speed at frequency ω, given by $\omega/\mathrm{Re}[k_s]$ where $k_s = \omega/c_s$ is the complex valued shear wave number, is related to the real (storage) and imaginary (loss) parts of the shear modulus, μ_R and μ_I, respectively, and the material density ρ as[35]

$$\frac{\omega}{\mathrm{Re}[k_s]} = \sqrt{\frac{2}{\rho}\frac{\mu_R^2 + \mu_I^2}{\mu_R + \sqrt{\mu_R^2 + \mu_I^2}}}. \tag{7}$$

Complex-valued surface (Rayleigh) wave number k_{Su} can be related to k_s through the following

$$k_{\mathrm{Su}} = k_s\frac{p}{\eta}. \tag{8}$$

In soft biological tissues, or cases where $|\lambda| \gg |\mu|$ we have that $|\eta/p| \approx 0.955$; but, due to the dispersive nature of viscoelastic materials there can be some slight variation of this ratio with frequency.

Note, the solution provided in Eq. (6a),[15] derived from the seminal works of Miller and Pursey[17,18] indicates that only Rayleigh waves are present on the surface of the half space in the steady state. However, other theoretical treatments have indicated that effects from compression and shear waves can also be felt at the surface via "head waves," at least under transient excitation conditions.[36–38] Given that all of this is linear system theory, it stands to reason that even in the steady state the effect of these head waves should be present, which may complicate the following analysis.

IV. ESTIMATING VISCOELASTIC PROPERTIES FROM SURFACE WAVE MEASUREMENTS

A. Approach 1: Measurement of surface wave speed as a function of frequency

The real part of the Rayleigh wave speed, or in effect the ratio of the circular frequency to the real part of the Rayleigh wavenumber $\mathrm{Re}[k_{\mathrm{Su}}]$, can be estimated from experimental measurements of the response to normal excitation[3] as described in Sec. III, as

$$\frac{\omega}{\mathrm{Re}[k_{Su}]} = \omega|\Delta r/\Delta\phi|, \tag{9}$$

where Δr is the distance of two measuring positions along a radial line away from the source of surface waves, $\Delta\phi$ is the wave phase change over this distance, and ω is the circular frequency in radians/second. Having measured phase speed at multiple frequencies via this approach, assuming $|p/\eta| = 1.05$, and by assuming a specific viscoelastic model type that expresses $\mu_R(\omega)$ and $\mu_I(\omega)$ in terms of unknown coefficients, one can then use Eq. (7) to optimize the values of these unknown coefficients to minimize the least square error between measured $\mathrm{Re}[k_{\mathrm{Su}}(\omega)]$ and calculated $\mathrm{Re}[k_{\mathrm{Su}}(\omega)]$. Given the nonlinear dependence of the value in Eq. (7) with respect to $\mu_R(\omega)$ and $\mu_I(\omega)$ it is expected that multiple local optima may exist and care must be taken in terms of an initial guess in the optimization routine. Theoretical, numerical and experimental example cases applications of this approach are described in the following Secs. V–VII below.

B. Approach 2: Measurement of the frequency response function

Measurement of the complex-valued frequency response function (FRF) between the driven oscillating disk and normal motion at a radial distance r from the center of the disk is accomplished as described in Sec. VII below. Referring to Eq. (6) and taking the ratio of the motion at the radial location r to that on the disk at radial location "a," we have

$$\mathrm{FRF} = \frac{u_z(r)}{u_z(a)} = \frac{K_0(jprk_p)}{K_0(jpak_p)} = \frac{K_0(jrk_{\mathrm{Su}})}{K_0(jak_{\mathrm{Su}})}. \tag{10}$$

Note, under the assumption that $|jak_{\mathrm{Su}}| \gg 1/4$ and using Bessel function asymptotic limits we have that

$$\mathrm{FRF} = \frac{u_z(r)}{u_z(a)} \approx \sqrt{\frac{a}{r}}e^{jk_{\mathrm{Su}}(a-r)}. \tag{11}$$

Asymptotic Eq. (11) clearly shows the geometric attenuation of the ratio of displacement amplitudes depending on radial distance r raised to the half power. Attenuation due to viscosity will manifest in the imaginary part of k_{Su}. In approach 2, the real and imaginary part of measured FRF (produced analytically, numerically, or experimentally) are fit with Eq. (10) in a least square error sense. First p is calculated from the fitting. From Eq. (6c) η is solved. Multiple solutions exist in Eq. (6c), but the only η that makes sense is the one whose real part is slightly smaller in amplitude than that of p as the surface wave speed is a slightly less than the shear wave speed. The complex shear modulus is calculated from Eq. (6d). Finally, the viscoelastic parameters (except for the static shear modulus μ_0 for each model assumed to be measured statically) are estimated by fitting μ_{R}, μ_I/ω based on the assumed viscoelastic model, such as fractional Voigt [Eqs. (4a) and (4b)], or SLS [Eqs. (5a) and (5b)]. Here, μ_I/ω is listed instead of μ_I as a way to quickly assess the appropriateness of the integer Voigt model (μ_I/ω independent of frequency). And, μ_0 is chosen to be the actual value used in the analytical or numerical study or statically measured in the experimental study. Theoretical, computational and

TABLE I. Viscoelastic material models used in analytical and numerical case studies.

	Voigt ($\alpha = 1$)	Fractional Voigt	SLS ($\alpha = 1$)
μ_0 (kPa)	23.9	14.0	14.0
μ_α (Pa.s$^\alpha$)	6.60	140	12.0
	–	$\alpha = 0.60$	$\mu_\omega = 16.0$ kPa

experimental example cases studies are described in Secs. V–VII below.

C. Initial comparison of approaches 1 and 2

The inherent difference between the two approaches described above is that, while the 1st approach only uses the measured surface wave speed as a function of frequency, the 2nd approach effectively uses both the surface wave speed and attenuation as a function of frequency. Thus, one may expect that the 2nd approach will provide more information in terms of both helping to determine the appropriate viscoelastic model *type,* as well as the optimal coefficient values for that type. However, in terms of practical implementation, it may be more difficult to acquire accurate measurements of attenuation, especially given that the above analyses are predicated on the fictional notion of an infinite halfspace. Actual applications will involve finite boundaries, and the possibility of the contamination of the FRF with other wave types, e.g., compression waves, and multi-path reflections. Of course, these complexities may also affect the accuracy of approach 1.

V. ANALYTICAL CASE STUDIES

A. Optimal model identification procedures

With each of the material cases depicted in Table I, consider a halfspace of a linear viscoelastic isotropic material with density $\rho = 1000\,\text{kg/m}^3$. Consider that surface wave excitation is initiated via a disk of radius $a = 1$ cm over the frequency range of 100–600 Hz as envisioned in Sec. III and that phase speed is determined per Eq. (9), and the FRF is determined per Eq. (10). The FRF is plotted for two frequencies in Fig. 3. Approaches 1 and 2 of the previous section are used to identify the optimal coefficients for an assumed viscoelastic model using response data at 11 frequencies spaced in 50 Hz increments from 100 to 600 Hz.

Specifically, per approach 1, it is assumed that μ_0 is already known from a static indentation measurement. Using Eq. (7) and assuming a Voigt model, in MATLAB™ the createOptimProblem and GlobalSearch commands are used to optimize the estimate of μ_1 to minimize the error between

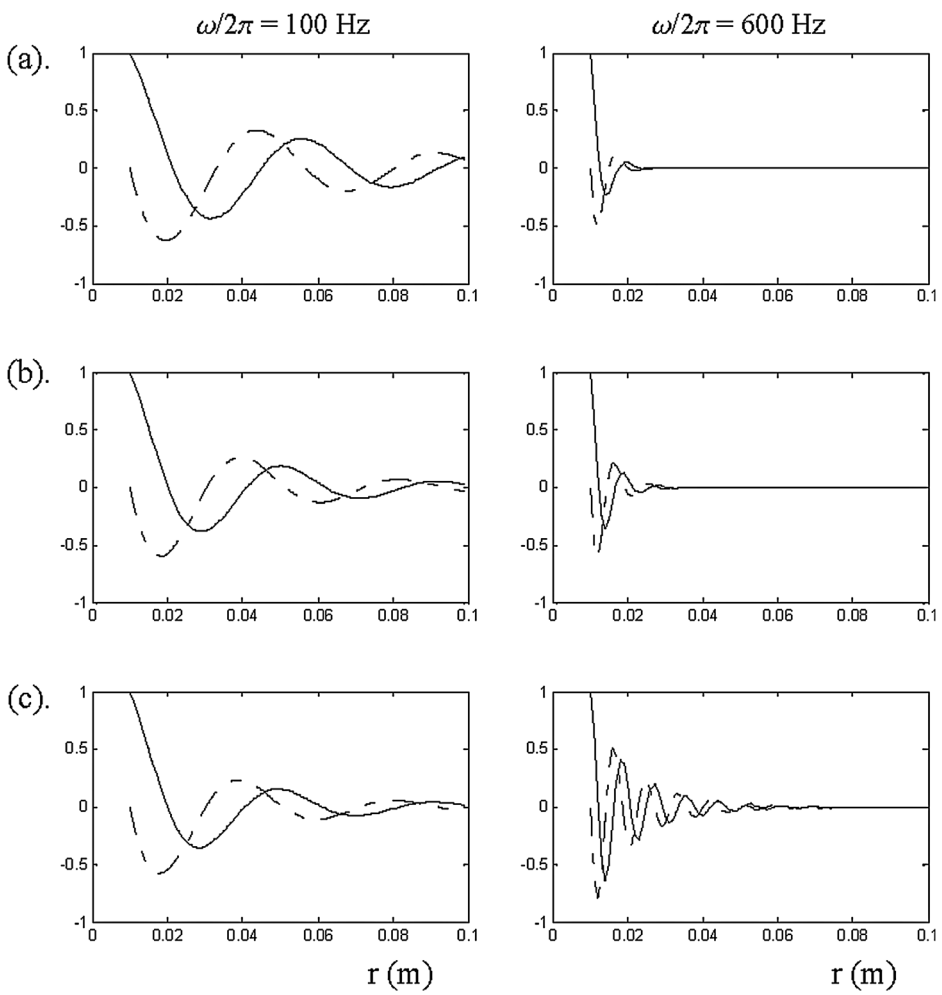

FIG. 3. Theoretical Studies. FRF at $\omega/2\pi = 100$ and 600 Hz for (a) Voigt, (b) fractional Voigt, and (c) SLS material studies. Key: —, real part; - · -, imaginary part. Material property values given in Table I.

TABLE II. Estimated viscoelastic coefficients and residual error in analytical case studies.

Approach 1							Approach 2						
				Residual Error ($\times 10^3$)							Residual Error ($\times 10^3$)		
				μ_R	μ_I	μ					μ_R	μ_I	μ
Actual material: Voigt							Actual material: Voigt						
Voigt	μ_0[kPa]	μ_1[Pa.s]		0	0.4	0.4	Voigt	μ_0[kPa]	μ_1[Pa.s]		0	0	0
	23.9	6.66						23.9	6.6				
Fractional	μ_0[kPa]	μ_α[Pa.s$^\alpha$]	α	0.3	0.34	0.4	Fractional	μ_0[kPa]	μ_α[Pa.s$^\alpha$]	α 1	0	0	0
Voigt	23.9	6.86	0.99				Voigt	23.9	6.6				
SLS	μ_0[kPa]	μ_ω[kPa]	μ_1[Pa.s]	1.4	0.028	1.4	SLS	μ_0[kPa]	μ_ω[kPa]	μ_1[Pa.s]	0	0	0
	23.9	741	6.5					23.9	1e6	6.6			
Actual material: Fractional Voigt							Actual material: Fractional Voigt						
Voigt	μ_0[kPa]	μ_1[Pa.s]		27	14	30	Voigt	μ_0[kPa]	μ_1[Pa.s]		27	8	29
	14	6.4						14	5.62				
Fractional	μ_0[kPa]	μ_α[Pa.s^a]	α	0.2	0.3	0.4	Fractional	μ_0[kPa]	μ_α[Pa.s$^\alpha$]	α	0	0	0
Voigt	14	141.7	0.59				Voigt	14	140	0.6			
SLS	μ_0[kPa]	μ_ω[kPa]	μ_1[Pa.s]	8	8	12	SLS	μ_0[kPa]	μ_ω[kPa]	μ_1[Pa.s]	2	25	5
	14	21.8	8.9					14	11.6	9.69			
Actual material: SLS							Actual material: SLS						
Voigt	μ_0[kPa]	μ_1[Pa.s]		36	31	48	Voigt	μ_0[kPa]	μ_1[Pa.s]		36	18	40
	14	6						14	4.17				
Fractional	μ_0[kPa]	μ_α[Pa.s$^\alpha$]	α	5	6	9	Fractional	μ_0[kPa]	μ_α[Pa.s$^\alpha$]	α	2.9	36	37
Voigt	14	808	0.36				Voigt	14	151	0.63			
SLS	μ_0[kPa]	μ_ω[kPa]	μ_1[Pa.s]	0.3	0.2	0.4	SLS	μ_0[kPa]	μ_ω[kPa]	μ_1[Pa.s]	0	0	
	14	16.1	12.08					14	16	12			

measured and calculated phase speeds in a least square error sense (summing the squares of the difference between the calculated and measured phase speed at each frequency). This processing is then repeated but instead assuming a Fractional Voigt model or a SLS model. In the case of the Fractional Voigt model, estimates of α and μ_α are optimized. For the SLS model assumption, estimates of μ_ω and μ_1 are optimized.

Per approach 2, it is also assumed that μ_0 is already known from a static indentation measurement. First assuming a Voigt model, the same MATLAB commands are used to optimize an estimate of μ_1 to minimize the error between measured and calculated $\mu_R(\omega)$ and $\mu_I(\omega)/\omega$ (summing the squares of the difference between the calculated and measured values of $\mu_R(\omega)$ and $\mu_I(\omega)/\omega$). In the case of the Fractional Voigt model, estimates of α and μ_α are optimized.

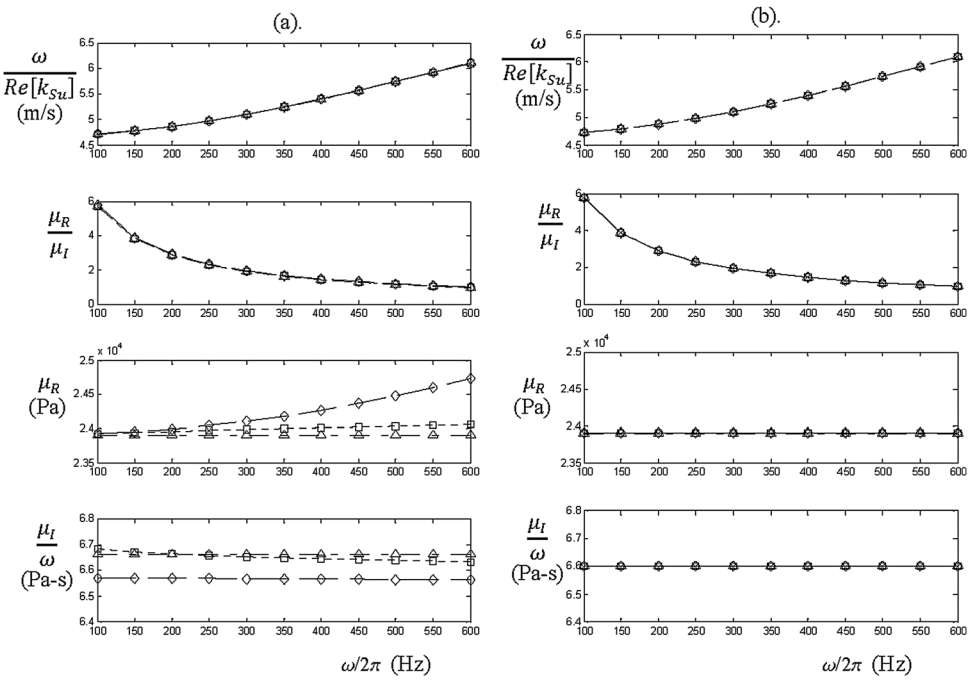

FIG. 4. Voigt material study. Best fit Voigt, fractional Voigt, and SLS models based on (a) Approach 1 and (b) Approach 2. Key: **x x x**, actual value; —, estimated value based on Approach 1 (ω/Re[k_{Su}]) or Approach 2 (μ_R and μ_I); △ - - - △, best fit Voigt; □·····□, best fit fractional Voigt; ◇ - - - ◇, best fit SLS.

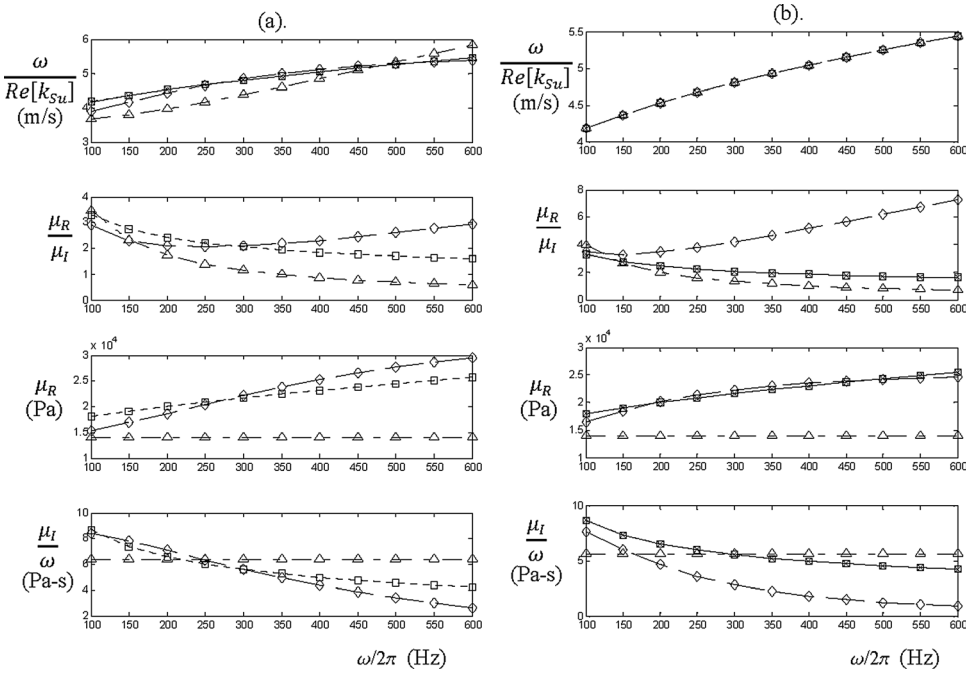

FIG. 5. Fractional Voigt material study. Best fit Voigt, fractional Voigt, and SLS models based on (a) approach 1 and (b) approach 2. Key: **x x x**, actual value; —, estimated value based on approach 1 ($\omega/\mathrm{Re}[k_{\mathrm{Su}}]$) or approach 2 ($\mu_R$ and μ_I); △ - · - △, best fit Voigt; □·····□, best fit fractional Voigt; ◇ - - - ◇, best fit SLS.

Finally estimates of μ_ω and μ_1 are optimized for the SLS model assumption.

B. RESULTS AND DISCUSSION

Results of the best fits using approaches 1 and 2 are provided in Table II and in Figs. 4–6. Referring to Table II, it is seen that approach 2 generally outperforms approach 1, minimizing error to machine tolerance when the appropriate model type is selected. It may also be observed from the figures that, generally, being able to compare estimates of $\mu_R(\omega)$ and $\mu_I(\omega)/\omega$ to measured values more clearly identifies *which* viscoelastic model type is appropriate, relative to comparing estimates of phase speed to measured values. (Note, for the Voigt material model, approach 2 correctly drives the fractional Voigt and SLS models to that of a Voigt model by driving α to 1 and μ_ω to the upper limit allowed in the optimization routine, respectively.)

VI. NUMERICAL CASE STUDIES

A. FE simulation cases

The three material property cases of the previous section are next simulated in a finite element (FE) environment using harmonic analysis, except with the important caveat

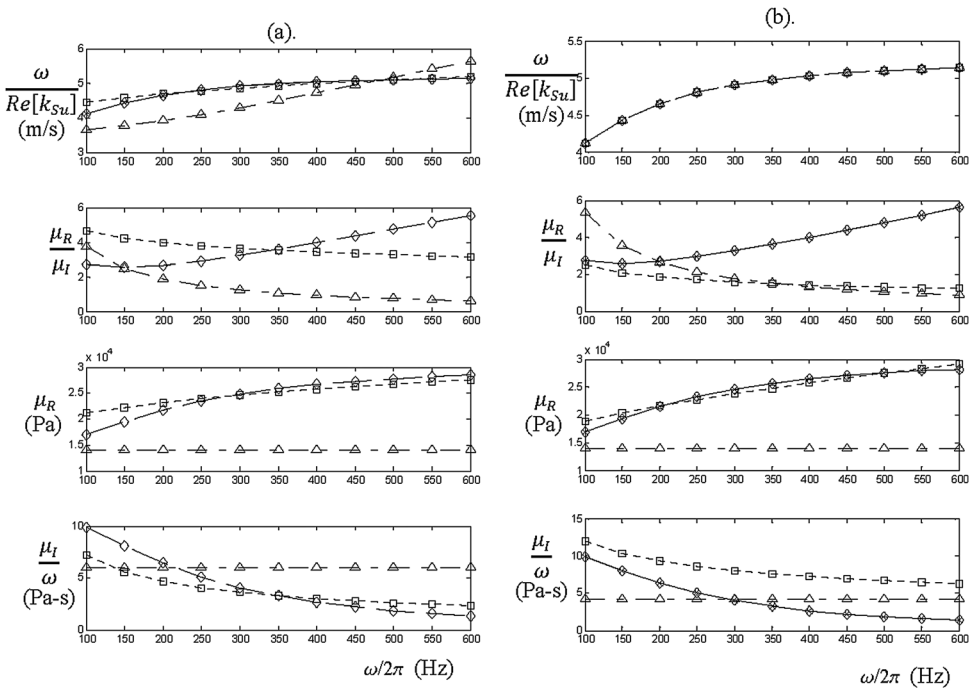

FIG. 6. SLS material study. Best fit Voigt, fractional Voigt, and SLS models based on (a) approach 1 and (b) approach 2. Key: **x x x**, actual value; —, estimated value based on approach 1 ($\omega/\mathrm{Re}[k_{\mathrm{Su}}]$) or approach 2 ($\mu_R$ and μ_I); △ - · - △, best fit Voigt; □·····□, best fit fractional Voigt; ◇ - - - ◇, best fit SLS.

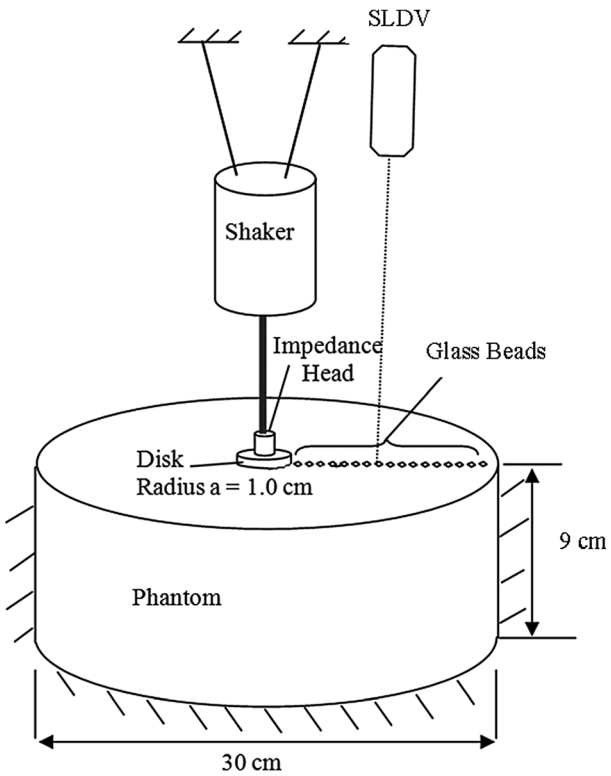

FIG. 7. Experimental schematic for measurement of surface wave motion caused by a surface source using a scanning laser Doppler vibrometer (SLDV).

that we no longer have an infinite half space. Rather, we have a cylinder of material, as depicted in Fig. 7, with finite boundaries. This can be treated as an axisymmetric problem in FE analysis. A 4 node quadrilateral element in the COMSOL® 4.2 structural mechanics module was used to generate the FRF (displacement/displacement) shown in Fig. 8. Studies with various element resolutions and other types (e.g., plane triangular element) confirmed that we had asymptotically reached a solution independent of element size/type. (Complementary studies conducted in ANSYS 11.0 that matched the COMSOL results but are not presented here, further verified the numerical approach taken.) While the theoretical analysis of the previous section was for a disk imparting a uniform pressure, a uniform displacement rather than uniform pressure was imparted because: (1) differences in FRFs between the two approaches appeared minimal, and (2) uniform displacement loading is closer to the actual loading in the experimental study in Sec. VII. In the FE solutions, the following parameter values were held constant: density $\rho = 1000\,\mathrm{kg/m^3}$ and bulk modulus $K = 2.6\,\mathrm{GPa}$. The viscoelastic coefficients of each model listed in Table I are specified, per Eqs. (4a), (4b), (5a), and (5b), which relate them to the complex shear modulus, $\mu = \mu_R + j\mu_I$, another input parameter in the FE simulation.

Due to finite boundaries and possibly head wave effects mentioned in the previous section, FE simulations do not result in the same FRF responses predicted by theory.

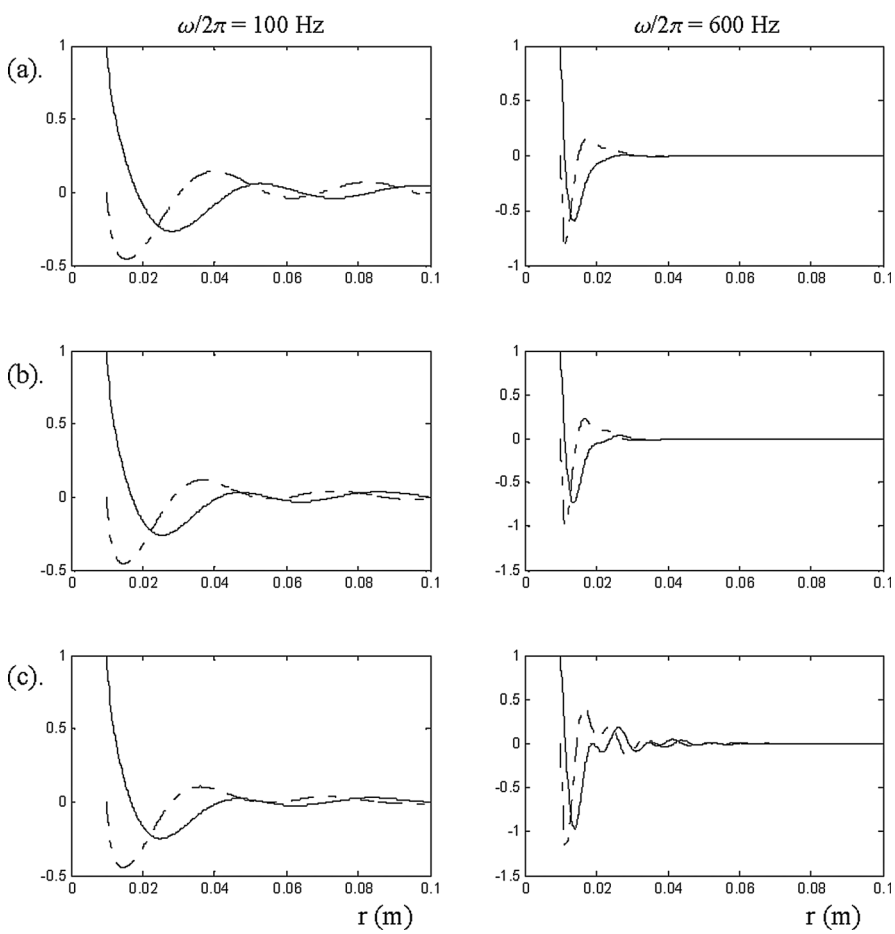

FIG. 8. Numerical studies. FRF at $\omega/2\pi = 100$ and 600 Hz for (a) Voigt, (b) fractional Voigt, and (c) SLS material studies. Key: —, real part; - · -, imaginary part. Material property values given in Table I.

TABLE III. Estimated viscoelastic coefficients and residual error in Numerical Case Studies.

Approach 1							Approach 2						
				Residual Error ($\times 10^5$)							Residual Error ($\times 10^5$)		
				μ_R	μ_I	μ					μ_R	μ_I	μ
Actual material: Voigt							Actual material: Voigt						
Voigt	μ_0[kPa]	μ_I[Pa.s]		0	4.6	4.6	Voigt	μ_0[kPa]	μ_I[Pa.s]		0	0.02	0.02
	23.9	81.7						23.9	6.94				
Fractional Voigt	μ_0[kPa]	μ_α[Pa.s$^\alpha$]	α	0	4.6	4.6	Fractional Voigt	μ_0[kPa]	μ_α[Pa.s$^\alpha$]	α	0	0.02	0.02
	23.9	81.7	1					23.9	6.94	1			
SLS	μ_0[kPa]	μ_ω[kPa]	μ_I[Pa.s]	0.1	4.6	4.6	SLS	μ_0[kPa]	μ_ω[kPa]	μ_I[Pa.s]	0	0.02	0.02
	23.9	1e6	81.7					23.9	1e6	6.86			
Actual material: Fractional Voigt							Actual material: Fractional Voigt						
Voigt	μ_0[kPa]	μ_I[Pa.s]		0.23	5.7	5.7	Voigt	μ_0[kPa]	μ_I[Pa.s]		0.27	0.1	0.29
	14	98.7						14	5.88				
Fractional Voigt	μ_0[kPa]	μ_α[Pa.s$^\alpha$]	α	0.23	5.7	5.7	Fractional Voigt	μ_0[kPa]	μ_α[Pa.s$^\alpha$]	α	0.11	0.07	0.13
	14	98.7	1					14	36.78	0.77			
SLS	μ_0[kPa]	μ_ω[kPa]	μ_I[Pa.s]	0.10	5.7	5.7	SLS	μ_0[kPa]	μ_ω[kPa]	μ_I[Pa.s]	0.11	0.06	0.12
	14	1e6	98.7					14	42	6.6			
Actual material: SLS							Actual material: SLS						
Voigt	μ_0[kPa]	μ_I[Pa.s]		0.30	0.40	0.50	Voigt	μ_0[kPa]	μ_I[Pa.s]		0.36	0.26	0.45
	14	9.3						14	5.42				
Fractional Voigt	μ_0[kPa]	μ_α[Pa.s$^\alpha$]	α	0.32	0.11	0.35	Fractional Voigt	μ_0[kPa]	μ_α[Pa.s$^\alpha$]	α	0.13	0.23	0.27
	14	9.7	0.1					14	75	0.67			
SLS	μ_0[kPa]	μ_ω[kPa]	μ_I[Pa.s]	0.32	0.09	0.33	SLS	μ_0[kPa]	μ_ω[kPa]	μ_I[Pa.s]	0.12	0.17	0.21
	14	21.5	61.7					14	26	7.2			

Likely, other wave types or wave reflections are present to varying degrees at different radial distances, which will alter predictions of the viscoelastic model based on approaches 1 and 2. Further analysis of the FE simulation data and calculation of best fit viscoelastic models per approaches 1 and 2 are conducted as described below.

B. Results and discussion

Results of the best fits using approaches 1 and 2 are provided in Table III and in Figs. 9–11. In comparing Figs. 9–11 (FEA) with Figs. 4–6 (theory), it becomes clear that the matter of extracting the correct viscoelastic model type and associated material property values based on surface

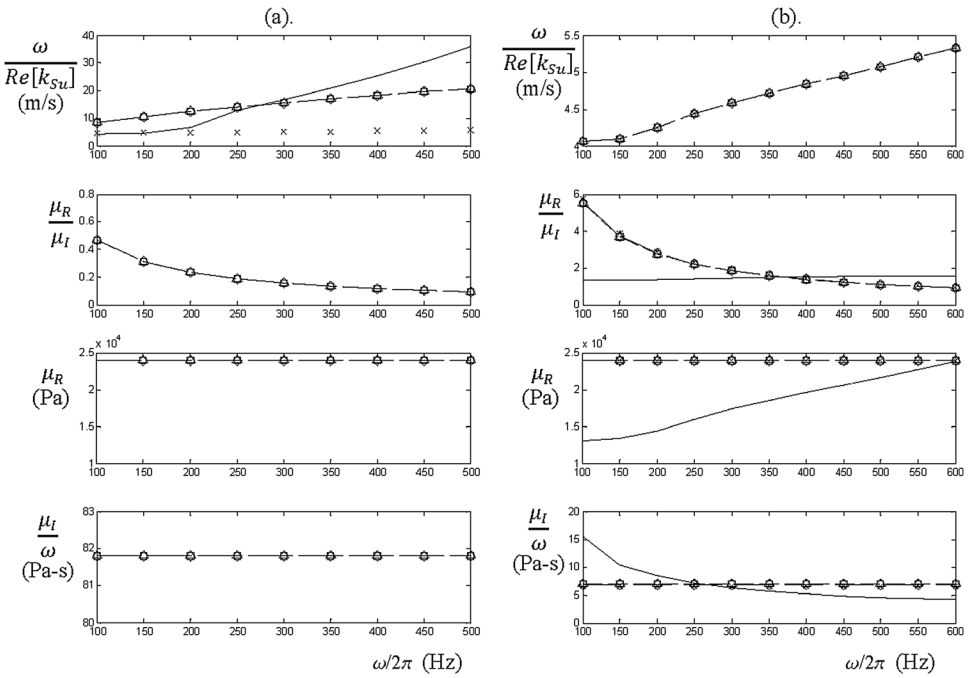

FIG. 9. Voigt numerical study. Best fit Voigt, fractional Voigt, and SLS models based on (a) approach 1 and (b) approach 2. Key: **x x x**, actual value; —, estimated value based on approach 1 ($\omega/\mathrm{Re}[k_{Su}]$) or approach 2 ($\mu_R$ and μ_I); △ - · - △, best fit Voigt; □·····□, best fit fractional Voigt; ◇ - - - ◇, best fit SLS.

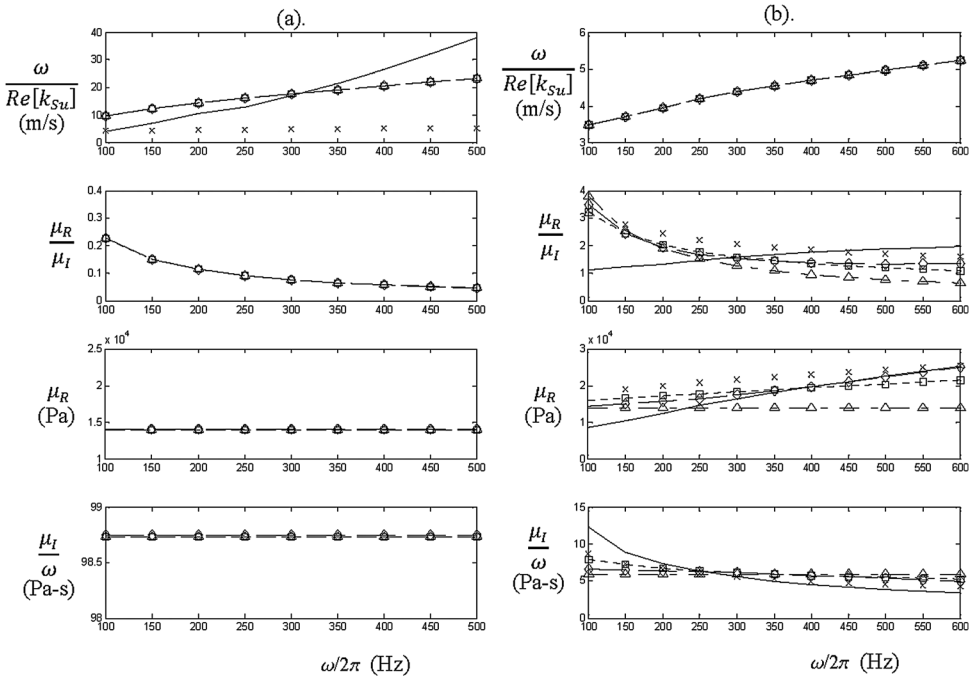

FIG. 10. Fractional Voigt numerical study. Best fit Voigt, fractional Voigt, and SLS models based on (a) approach 1 and (b) approach 2. Key: **x x x**, actual value; —, estimated value based on approach 1 ($\omega/\mathrm{Re}[k_{\mathrm{Su}}]$) or approach 2 ($\mu_R$ and μ_I); △ - · - △, best fit Voigt; □·····□, best fit fractional Voigt; ◊ - - - ◊, best fit SLS.

motion measurements is more challenging than the infinite half-space theory would suggest. From approach 1 for the Voigt and fractional Voigt cases, a Voigt model assumption essentially yields the best fit as the fractional Voigt and SLS optimizations converge to the Voigt case ($\alpha = 1$ and μ_ω large). For the SLS case, the SLS model assumption fits the phase speed well only from 100 to 300 Hz. This shows the limitation of approach 1 and the complexity caused by the finite boundary as the calculated phase speed based on Eq. (9) is not that accurate. From approach 2, the best fit model is usually the correct one except for the fractional Voigt case, where the SLS model does slightly better. For the Voigt model case, both the fractional Voigt and SLS models converge to the Voigt model as seen from their respective estimated parameters. For the SLS case, the SLS model is the best fit as the residual error of the estimated shear modulus relative to the actual shear modulus is the smallest.

VII. EXPERIMENTAL STUDY

A. Experimental approach

Surface wave experiments were conducted as depicted in Fig. 7 on a silicone polymer, Ecoflex 00-10 (NuSil Technology, Carpinteria, CA), which had a density of 965 kg/m^3 calculated through basic mass volume measurements of small test specimens. While in liquid form, the material is

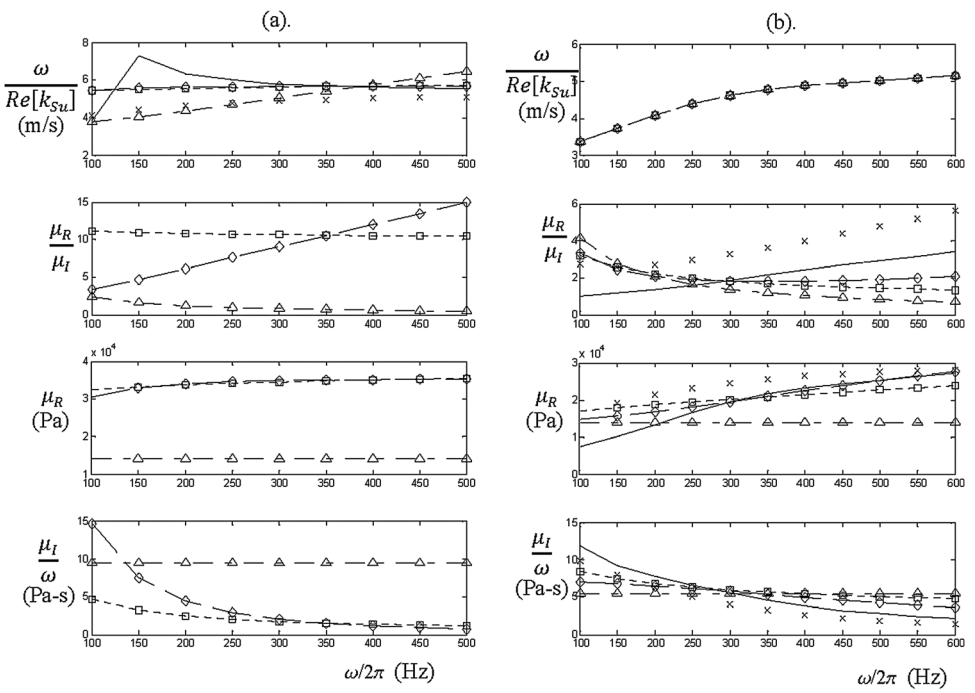

FIG. 11. SLS numerical study. Best fit Voigt, fractional Voigt, and SLS models based on (a) approach 1 and (b) approach 2. Key: **x x x**, actual value; —, estimated value based on approach 1 ($\omega/\mathrm{Re}[k_{\mathrm{Su}}]$) or approach 2 ($\mu_R$ and μ_I); △ - · - △, best fit Voigt; □·····□, best fit fractional Voigt; ◊ - - - ◊, best fit SLS.

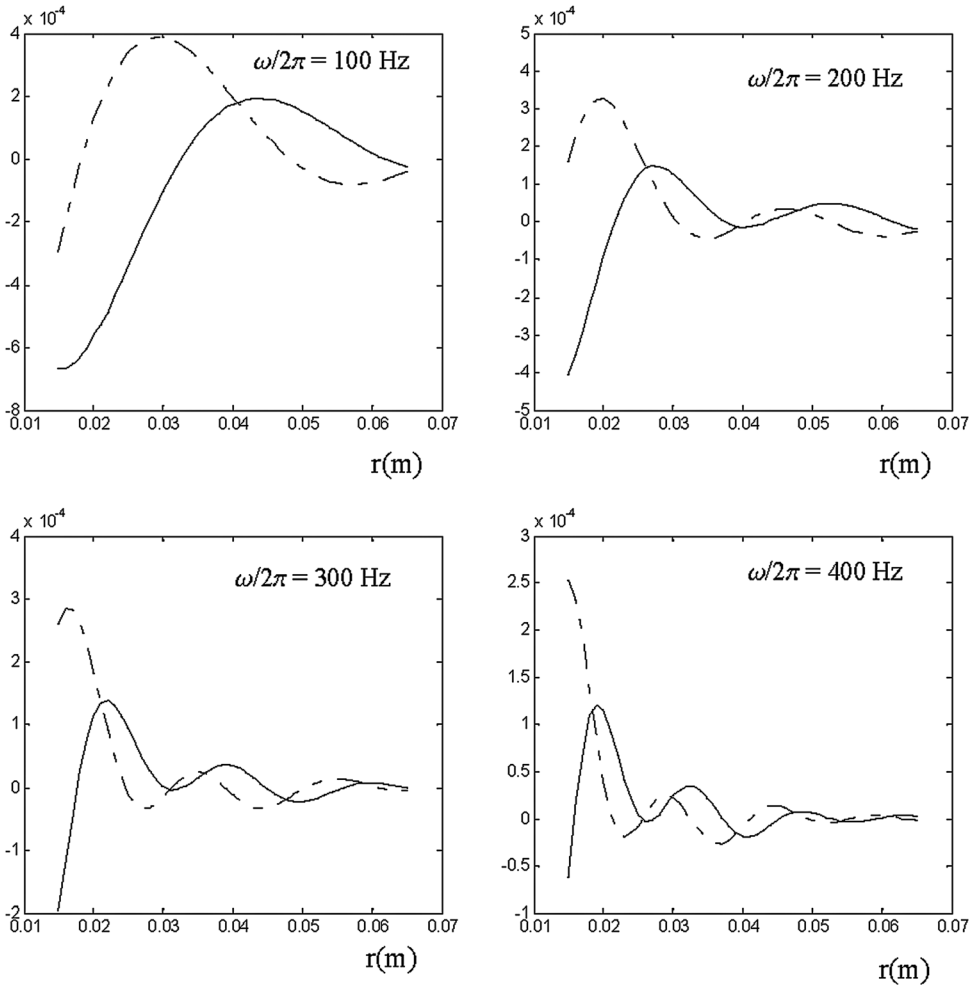

FIG. 12. Experimental study. FRF at $\omega/2 = 100, 200, \ldots, 600$ Hz. Key: —, real part; - · -, imaginary part.

poured into the container and then cures at room temperature. Once cured, the material is removed from the container and mounted on a vibration isolated optics bench. A plexiglass disk, driven by a mechanical shaker (ET-132, LabWorks Inc., Mesa Costa, CA) that is supported by a separate structure, is positioned on the surface of the phantom with a sufficient preload to ensure contact during excitation. The shaker is driven via an amplifier (Type 2076, Bruel & Kjaer, Denmark) with a signal input from a dynamic signal analyzer (35670 A, Agilent Technologies, Santa Clara, CA). The force and acceleration of the disk is measured with an impedance head (288D01, PCB Piezotronics, Depew, NY), and the out-of-plane velocity at discrete points on the surface are measured using a scanning laser Doppler vibrometer (SLDV) (PSV-400, Polytec, Irvine, CA). P-RETRO-250 glass beads (45–63 μm dia., Polytec, Irvine, CA) are spread on and adhered to the semi-translucent phantom material to aid in SLDV measurement. Scanning was along a line radially outward from the excitation over a distance of 50 mm with a 1 mm increment and the measurement point closest to

TABLE IV. Estimated viscoelastic coefficients and residual error in Experimental Studies.

Approach 1					Approach 2						
				Residual Error[a]					Residual Error ($\times 10^5$)[a]		
				Re [K_{su}]					μ_R	μ_I	μ
Voigt	μ_0[kPa]	μ_I[Pa.s]		66.19	Voigt	μ_0[kPa]	μ_I[Pa.s]		0.35	0.18	0.39
	13.3	11.77				13.3	9.96				
Fractional Voigt	μ_0[kPa]	μ_α[Pa.s$^\alpha$]	α	16.67	Fractional Voigt	μ_0[kPa]	μ_α[Pa.s$^\alpha$]	α	0.06	0.11	0.13
	13.3	535	0.49			13.3	350.77	0.55			
SLS	μ_0[kPa]	μ_ω[kPa]	μ_I[Pa.s]	17.19	SLS	μ_0[kPa]	μ_ω[kPa]	μ_I[Pa.s]	0.02	0.04	0.04
	13.3	29.5	18.97			13.3	27.25	17.77			

[a]Here, residual error is with respected to the calculated values of Re[K_{su}] (Approach 1) and complex μ (Approach 2), as the actual *values* and *type* of viscoelastic model are unknown.

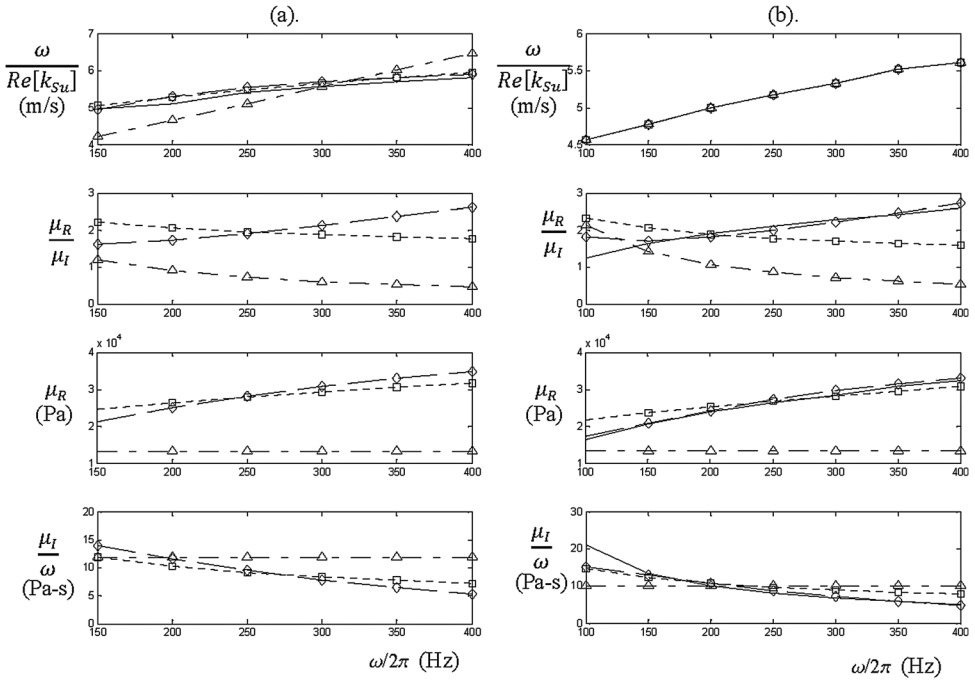

FIG. 13. Experimental study. Best fit Voigt, fractional Voigt, and SLS models based on (a) approach 1 and (b) approach 2. Key: —, estimated value; △ - · - △, best fit Voigt; □·····□, best fit fractional Voigt; ◊ - - - ◊, best fit SLS.

the excitation was 5 mm from the rim of the plexiglass disk. Measurement signals are recorded and the frequency response function (FRF) between the output (vertical velocity of the surface points) and input (motion input of the disk) is calculated by the dynamic signal analyzer. Measurements of FRF (velocity/acceleration) are shown in Fig. 12. The viscoelastic parameters estimation procedure here is essentially the same as the one for FE simulation.

A static measurement of the phantom material stiffness was made by indenting a steel sphere of diameter 9.525 mm into the media. Indentation forces were measured for different indentation depths using a force gauge (Model DPS, Imada, Northbrook, IL). Indentation of the steel ball into the semi-infinite medium was assumed to be a Hertzian contact problem and the solution given by Timoshenko[39] was used as described in Meral *et al.*[19] to estimate the static Young's modulus value, which could then be used to obtain an estimate of μ_0.

B. Results and discussion

Results of the best fits using approach 1 and 2 are shown in Table IV and Fig. 13. The phase speed estimated by approach 1 is plotted in a narrower frequency range than that by approach 2 as the phase speed measured between 100 Hz and 200 Hz deviated too much from the normally expected value. It is shown from Fig. 13(a) that by approach 1, a good match to frequency-dependent phase speed is possible for both the fractional Voigt and SLS model. This again leads to the same conclusion as in Sec. V that matching phase speed dispersion alone over an order or less of magnitude in frequency probably does not discern which model type is appropriate. While from Fig. 13(b), the more appropriate model can be identified from μ_R/μ_I versus frequency even though different models lead to almost the same fitting curves for phase speed, μ_R, and μ_I/ω. Thus one may be able to use approach 2 to better assess which model type is appropriate.

VIII. CONCLUSION

Two different approaches to identifying the type and coefficients of a viscoelastic model of a material based on surface wave measurements have been proposed. One approach has been to measure the Rayleigh wave speed as a function of frequency (i.e., wavelength as a function of frequency) and then to optimize the coefficients in an assumed viscoelastic model type to minimize the difference between the measured and predicted values. Another approach is to measure the complex-valued frequency response function (FRF) between the excitation location and points at known radial distances from the excitation location. (This does require that one knows the size and location of the excitation relative to the measurement points, information not necessary for the first approach.) The FRF has embedded in it frequency-dependent information about both surface wave phase speed (i.e., wavelength) and attenuation; it can be used to directly estimate the real and imaginary parts of the complex shear modulus (storage and loss shear moduli). The coefficients in an assumed viscoelastic tissue model type can then be optimized to minimize the differences in the predicted and experimentally determined values of the complex moduli. The relative merits of these approaches were explored theoretically, computationally and experimentally. While theoretical and experimental studies suggested that approach 2 was more capable of distinguishing which type of viscoelastic model was most appropriate, finite element studies highlighted the complications that arise due to finite boundary conditions and multiple wave types for both approaches. There are inherent limitations to identifying

viscoelastic properties based on surface wave measurements. The findings of this study on *surface* waves, in terms of the merits of different approaches and limitations, are likely also relevant to identification of viscoelastic models and properties based on *shear* wave imaging, given the close relationship between the two wave types.

ACKNOWLEDGMENT

The financial support of the National Institutes of Health (Grant Nos. EB012142 and EB007537) is acknowledged.

[1]Y. Yamakoshi, J. Sato, and T. Sato, "Ultrasonic imaging of internal vibration of soft tissue under forced vibration," IEEE Trans. Ultrason. Ferroelectr. Freq. Control **37**, 45–53 (1990).
[2]R. Muthupillai, D. J. Lomas, P. J. Rossman, J. F. Greenleaf, A. Manduca, and R. L. Ehman, "Magnetic resonance elastography by direct visualization of propagating acoustic strain waves," Science **269**, 1854–1857 (1995).
[3]X. M. Zhang, and J. F. Greenleaf, "Estimation of tissue's elasticity with surface wave speed," J. Acoust. Soc. Am. **122**, 2522–2525 (2007).
[4]F. A. Duck, *Physical Properties of Tissue: A Comprehensive Reference Book* (Academic Press, New York, 1990), pp. 225–229, Table VII.5; pp. 279–317, Table VIII.1 for T1, Table VIII.5 for T2.
[5]V. Kuperman, *Magnetic Resonance Imaging: Physical Principles and Applications* (Academic Press, New York, 2000), pp. 57–76, Table IV.1.
[6]K. Hoyt, T. Kneezel, B. Castaneda, and K. J. Parker, "Quantitative sonoelastography for the in vivo assessment of skeletal muscle viscoelasticty," Phys. Med. Biol. **53**, 4063–4080 (2008).
[7]Y. C. Fung, *Biomechanics: Mechanical Properties of Living Tissues*, 2nd ed. (Springer-Verlag, New York, 1993), pp. 336–343.
[8]A. P. Sarvazyan, O. V. Rudenko, S. D. Swanson, J. B. Fowlkes, and S. Y. Emelianov, "Shear wave elasticity imaging: A new ultrasonic technology of medical diagnostics," Ultrasound Med. Biol. **24**, 1419–1435 (1998).
[9]R. W. Chan and I. R. Titze, "Effect of postmortem changes and freezing on the viscoelastic properties of vocal fold tissues," Ann. Biomed. Eng. **31**, 482–491 (2003).
[10]D. Craiem and R. Armentano, "A fractional derivative model to describe arterial viscoelasticity," Biorheology **44**, 251–263 (2007).
[11]M. Z. Kiss, T. Varghese, and T. J. Hall, "Viscoelastic characterization of in vitro canine tissue," Phys. Med. Biol. **49**, 4207–4218 (2004).
[12]D. Klatt, U. Hamhaber, P. Asbach, J. Braun, and I. Sack, "Noninvasive assessment of the rheological behavior of human organs using multifrequency MR elastography: A study of brain and liver viscoelasticity," Phys. Med. Biol. **52**, 7281–7294 (2007).
[13]K. Riek, D. Klatt, H. Nuzha, S. Mueller, U. Neumann, I. Sack, and J. Braun, "Wide-range dynamic magnetic resonance elastography," J. Biomech. **44**, 1380–1386 (2011).
[14]R. Sinkus, K. Siegmann, T. Xydeas, M. Tanter, C. Claussen, and M. Fink, "MR Elastography of breast lesions: Understanding the solid/liquid duality can improve the specificity of contrast-enhanced MR mammography," Mag. Reson. Med. **58**, 1135–1144 (2007).
[15]T. J. Royston, H. A. Mansy, and R. H. Sandler, "Excitation and propagation of surface waves on a viscoelastic half-space with application to medical diagnosis," J. Acoust. Soc. Am. **106**, 3678–3686 (1999).
[16]T. J. Royston, Y. Yazicioglu, and F. Loth, "Surface response of a viscoelastic medium to subsurface acoustic sources with application to medical diagnosis," J. Acoust. Soc. Am. **113**, 1109–1121 (2003).
[17]G. F. Miller and H. Pursey, "The field and radiation impedance of mechanical radiators on the free surface of a semi-infinite isotropic solid," Proc. R. Soc. A **223**, 521–541 (1954).
[18]G. F. Miller and H. Pursey, "On the partition of energy between elastic waves in a semi-infinite solid," Proc. R. Soc. A **223**, 55–69 (1955).
[19]F. C. Meral, T. J. Royston, and R. L. Magin, "Surface response of a fractional order viscoelastic halfspace to surface and subsurface sources," J. Acoust. Soc. Am. **126**, 3278–3285 (2009).
[20]X. M. Zhang, R. R. Kinnick, and J. F. Greenleaf, "Viscoelasticity of lung tissue with surface wave method," *Ultrasonics Symposium, 2008. IUS 2008. IEEE*, pp. 21–23 (2008).
[21]B. Qiang, J. F. Greenleaf, and X. M. Zhang, "Quantifying viscoelasticity of gelatin phantoms by measurement impulse response using compact optical sensors," IEEE Trans. Ultrason. Ferroelectr. Freq. Control **57**, 1696–1700 (2010).
[22]X. M. Zhang, T. G. Osborn, M. R. Pittelkow, B. Qiang, R. R. Kinnick and J. F. Greenleaf, "Quantitative assessment of scleroderma by surface wave technique," Med. Eng. Phys. **33**, 31–37 (2011).
[23]S. G. Chen, M. Fatemi, and J. F. Greenleaf, "Quantifying elasticity and viscosity from measurement of shear wave speed dispersion," J. Acoust. Soc. Am. **115**, 2781–2785 (2004).
[24]X. M. Zhang, R. R. Kinnick, M. Fatemi, and J. F. Greenleaf, "Noninvasive method for estimation of complex elastic modulus of arterial vessels," IEEE Trans. Ultrason. Ferroelectr. Freq. Control **52**, 642–652 (2005).
[25]A. Giannoula and R. S. C. Cobbold, "Narrowband shear wave generation by a finite-amplitude radiation force: The fundamental component," IEEE Trans. Ultrason. Ferroelectr. Freq. Control **55**, 343–358 (2008).
[26]A. Giannoula and R. S. C. Cobbold, "Propagation of shear waves generated by a modulated finite amplitude radiation force in a viscoelastic medium," IEEE Trans. Ultrason. Ferroelectr. Freq. Control **56**, 575–588 (2009).
[27]T. Deffieux, G. Montaldo, M. Tanter, and M. Fink, "Shear wave spectroscopy for in vivo quantification of human soft tissues visco-elasticity," IEEE Trans. Med. Imag. **28**, 313–322 (2009).
[28]J. L. Gennisson, T. Deffieux, E. Macé, G. Montaldo, M. Fink, and M. Tanter, "Viscoelastic and anisotropic mechanical properties of in vivo muscle tissue assessed by supersonic shear imaging," Ultrasound Med. Biol. **36**, 789–801 (2010).
[29]M. Orescanin and M. F. Insana, "Shear modulus estimation with vibrating needle stimulation," IEEE Trans. Ultrason. Ferroelectr. Freq. Control **57**, 1358–1367 (2010).
[30]H. L. Oestreicher, "Field and impedance of an oscillating sphere in a viscoelastic medium with an application to biophysics," J. Acoust. Soc. Am. **23**, 707–714 (1951).
[31]R. L. Magin, *Fractional Calculus in Bioengineering* (Begell House, Redding, CT, 2006), pp. 269–355.
[32]N. Heymans, "Dynamic measurements in long-memory materials: Fractional calculus evaluation of approach to steady state," J. Vib. Control **14**, 1587–1596 (2008).
[33]F. Mainardi, "Fractional calculus: Some basic problems in continuum and statistical mechanics," in *Fractals and Fractional Calculus in Continuum Mechanics*, edited by A. Carpinteri and F. Mainardi (Springer-Verlag, New York, 1997), p. 291.
[34]R. S. Lakes, *Viscoelastic Solids* (CRC Press, Boca Raton, FL, 1999), pp. 31–36.
[35]S. F. Othman, H. Xu, T. J. Royston, and R. L. Magin, "Microscopic magnetic resonance elastography (μMRE)," Magn. Reson. Med. **54**, 605–614 (2005).
[36]Y. C. Fung, *Foundations of Solid Mechanics* (Prentice Hall, Englewood Cliffs, NJ, 1965), pp. 224–225.
[37]J. D. Achenbach, *Wave Propagation in Elastic Solids* (North-Holland, Amsterdam, 1973), p. 307.
[38]K. F. Graff, *Wave Motion in Elastic Solids* (Dover Publications, New York, 1991), p. 370.
[39]S. P. Timoshenko and J. N. Goodier, *Theory of Elasticity*, 3rd ed. (McGraw-Hill, New York, 1970), pp. 409–412.